NANO LETTERS

Letter

pubs.acs.org/NanoLett

Molecular Selectivity of Graphene-Enhanced Raman Scattering

Shengxi Huang,[†] Xi Ling,*[,†] Liangbo Liang,[‖] Yi Song,[†] Wenjing Fang,[†] Jin Zhang,[§] Jing Kong,[†] Vincent Meunier,[‖] and Mildred S. Dresselhaus*[,†,⊥]

[†]Department of Electrical Engineering and Computer Science, Massachusetts Institute of Technology, Cambridge, Massachusetts 02139, United States

[‖]Department of Physics, Applied Physics, and Astronomy, Rensselaer Polytechnic Institute, Troy, New York 12180, United States

[§]Center for Nanochemistry, Beijing National Laboratory for Molecular Sciences, Key Laboratory for the Physics and Chemistry of Nanodevices, State Key Laboratory for Structural Chemistry of Unstable and Stable Species, College of Chemistry and Molecular Engineering, Peking University, Beijing 100871, People's Republic of China

[⊥]Department of Physics, Massachusetts Institute of Technology, Cambridge, Massachusetts 02139, United States

Supporting Information

ABSTRACT: Graphene-enhanced Raman scattering (GERS) is a recently discovered Raman enhancement phenomenon that uses graphene as the substrate for Raman enhancement and can produce clean and reproducible Raman signals of molecules with increased signal intensity. Compared to conventional Raman enhancement techniques, such as surface-enhanced Raman scattering (SERS) and tip-enhanced Raman scattering (TERS), in which the Raman enhancement is essentially due to the electromagnetic mechanism, GERS mainly relies on a chemical mechanism and therefore shows unique molecular selectivity. In this paper, we report graphene-enhanced Raman scattering of a variety of different molecules with different molecular properties. We report a strong molecular selectivity for the GERS effect with enhancement factors varying by as much as 2 orders of magnitude for different molecules. Selection rules are discussed with reference to two main features of the molecule, namely its molecular energy levels and molecular structures. In particular, the enhancement factor involving molecular energy levels requires the highest occupied molecular orbital (HOMO) and lowest unoccupied molecular orbital (LUMO) energies to be within a suitable range with respect to graphene's Fermi level, and this enhancement effect can be explained by the time-dependent perturbation theory of Raman scattering. The enhancement factor involving the choice of molecular structures indicates that molecular symmetry and substituents similar to that of the graphene structure are found to be favorable for GERS enhancement. The effectiveness of these factors can be explained by group theory and the charge-transfer interaction between molecules and graphene. Both factors, involving the molecular energy levels and structural symmetry of the molecules, suggest that a remarkable GERS enhancement requires strong molecule−graphene coupling and thus effective charge transfer between the molecules and graphene. These conclusions are further experimentally supported by the change of the UV−visible absorption spectra of molecules when in contact with graphene and these conclusions are theoretically corroborated by first-principles calculations. These research findings are important for gaining fundamental insights into the graphene−molecule interaction and the chemical mechanism in Raman enhancement, as well as for advancing the role of such understanding both in guiding chemical and molecule detection applications and in medical and biological technology developments.

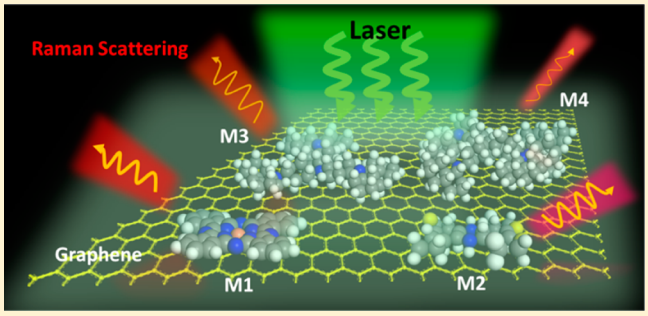

KEYWORDS: *Graphene-enhanced Raman scattering, molecular energy level, molecular structure, graphene−molecule interaction, chemical enhancement*

Surface-enhanced Raman scattering (SERS) is an important Raman enhancement technique in the study of the physics and chemistry of materials.[1−4] Noble metals with rough surfaces are typically used as SERS substrates.[5,6] The Raman enhancement processes are mainly due to the interplay between an electromagnetic mechanism (EM)[7] and a chemical mechanism (CM).[8] In the EM, the electromagnetic field of the incident light is enhanced by a plasmonic mechanism near the "hot spots" on the rough surface of a metal. In the CM, the substrate and the molecules are coupled through both charge transfer and the mixing of molecular orbitals with electronic states. In SERS, the dominant enhancement mechanism is the EM, and it can enhance the Raman signals by as much as 10^{10} times.[9] The enhancement factors (EFs) vary with the vibrational modes for both EM and CM, but they have

Received: November 30, 2014
Revised: March 20, 2015
Published: March 30, 2015

DOI: 10.1021/nl5045988
Nano Lett. 2015, 15, 2892−2901

different mechanisms. For EM, the variation of EF depends on the electromagnetic frequency resonance.[1,4] However, for CM, EF depends on the molecule−substrate interaction, showing a strong molecular selectivity. Investigating the molecular selectivity of SERS is very important to understand the CM in detail, which until now has been insufficiently explored to effectively provide a complete picture of the overall enhancement mechanisms of SERS.[1,10,11]

Graphene-enhanced Raman scattering (GERS), which uses graphene rather than a rough metal surface as a Raman enhancement surface, is a newly developed Raman enhancement technique.[12] GERS is dominated by the CM with associated EF values varying from less than 10 to as high as ∼100.[12,13] While a number of factors responsible for this EF have been successfully explained, such as the number of graphene layers,[14] the molecule−graphene distance,[15] molecular orientations,[16] Fermi level of graphene,[17] and laser excitation energies,[13] the molecular selectivity of graphene-enhanced Raman scattering has not yet been systematically explored.

Compared to SERS, GERS has a relatively lower EF. Although GERS has not demonstrated its detection limit down to the single molecule level up to now, its EF values can still be very useful and large enough in some applications for the detection of a small number of molecules. Thanks to the unique two-dimensional planar structure and the chemical inertness of graphene, GERS presents many advantages, such as the repeatability and stability of the enhanced Raman signal, when compared to conventional SERS.[13,18,19] Previous works have established that the GERS EFs vary with the type of molecules and the phonon modes within the same molecules.[12] In particular, some molecules can have GERS enhancement while others do not. Even for the same type of vibrational mode, different molecules can show different GERS EFs. Such a remarkable selectivity of molecules is very important for GERS to be a promising tool in microanalysis, as well as to gain a deep understanding of the CM. To predict which kinds of molecules have strong GERS enhancement and to provide a more comprehensive understanding of the CM in SERS, a systematic study of molecular selectivity of GERS is necessary.

The molecular selectivity of GERS originates from the different strengths of the interactions between graphene and different molecules.[8,10] van der Waals (vdW) forces govern most of the molecule−graphene interactions. In GERS, the different interaction strengths between the molecules and the graphene substrate contribute different values of GERS EFs. Therefore, the molecular selectivity of the GERS effect can be exploited to determine the coupling strength between graphene and the molecules.

A large Raman cross section of the molecule ensures sufficient Raman scattering efficiency and therefore the observation of clear Raman signals.[20] For this reason, we chose molecules with large Raman cross sections to investigate GERS capabilities for molecular selectivity. The Raman scattering of different types of molecules on graphene is shown in Figure 1. These molecules can be categorized as follows. Category (1) encompasses molecules with similar molecular structures but different energy levels and includes different phthalocyanine (Pc) derivatives: copper phthalocyanine (CuPc), zinc phthalocyanine (ZnPc), and Copper(II) 1,2,3,4,8,9,10,11,15,16,17,18,22,23,24,25-hexadecafluoro-29H,31H-phthalocyanine (F_{16}CuPc). Category (2) involves molecules with similar energy levels but different molecular

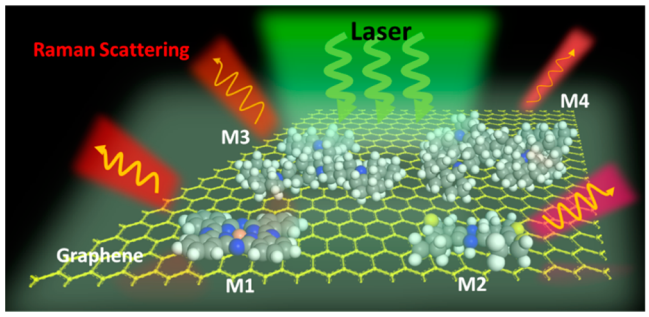

Figure 1. Schematic illustration of the molecular selectivity in GERS. Different types of molecules M1, M2, M3, and M4 are shown on graphene.

structures, such as tetrathienophenazine (TTP), tris(4-carbazoyl-9-ylphenyl) amine (TCTA), and 2,2′,7,7′-tetra(*N*-phenyl-1-naphthyl-amine)-9,9′-spirobifluorene (sp2-NPB). Finally, category (3) includes other molecules of interest, such as 3,5-tris(*N*-phenylbenzimiazole-2-yl)benzene (TPBi), bathocuproine (BCP), and so forth.

We analyzed the enhancement effects of all these molecules on graphene and could highlight two molecular selection rules. First, molecular energy levels play an important role in determining whether or not a significant enhancement effect can be observed. We find that the highest occupied molecular orbital (HOMO) and lowest unoccupied molecular orbital (LUMO) levels of the molecule need to be in the appropriate energy range with respect to graphene's Fermi level for a given set of laser excitation energies. This rule is supported by the experimental results and theoretical analyses using the third order perturbation theory in the quantum theory of Raman scattering.[21] The second selection rule is that the symmetry of the molecule is important in showing a considerable enhancement effect. The molecules which show symmetries closest to that of graphene symmetry (D_{6h}) are more likely to yield a large GERS EF. This molecular symmetry rule, confirmed by Raman measurement results using molecules with different structures, can be theoretically explained by group theory and the charge-transfer effect between the molecules and graphene. Both molecular selection rules for the molecular energy levels and for the molecular symmetry suggest that a strong GERS EF requires both strong molecule−graphene coupling and effective charge transfer, which are further supported by the UV−visible absorption spectroscopy measurement of molecules before and after contacting graphene surfaces. First-principles density functional theory (DFT) calculations were also carried out to confirm the sensitive dependence of GERS EF on the molecular HOMO/LUMO levels and on the molecule−graphene coupling. The rules of molecular selectivity in a GERS system explored in our work are important for the fundamental study of the CM in GERS and of the graphene−molecule interaction, as well as the potential application of GERS in molecular detection and biological, physical, and chemical process monitoring.[22−27]

Results and Discussions. Selection of the type of molecules is essential in GERS experiments. In previous reports, most of the studied molecules have large Raman cross sections, including protoporphyin IX, crystal violet, Rhodamine 6G, and Pc and its derivatives.[12] However, many molecules that we tested in the GERS experiments did not show Raman signals because of the low Raman cross section (smaller than 10^{-30} cm^2 sr^{-1} under nonresonant conditions,[20]

DOI: 10.1021/nl5045988
Nano Lett. 2015, 15, 2892−2901

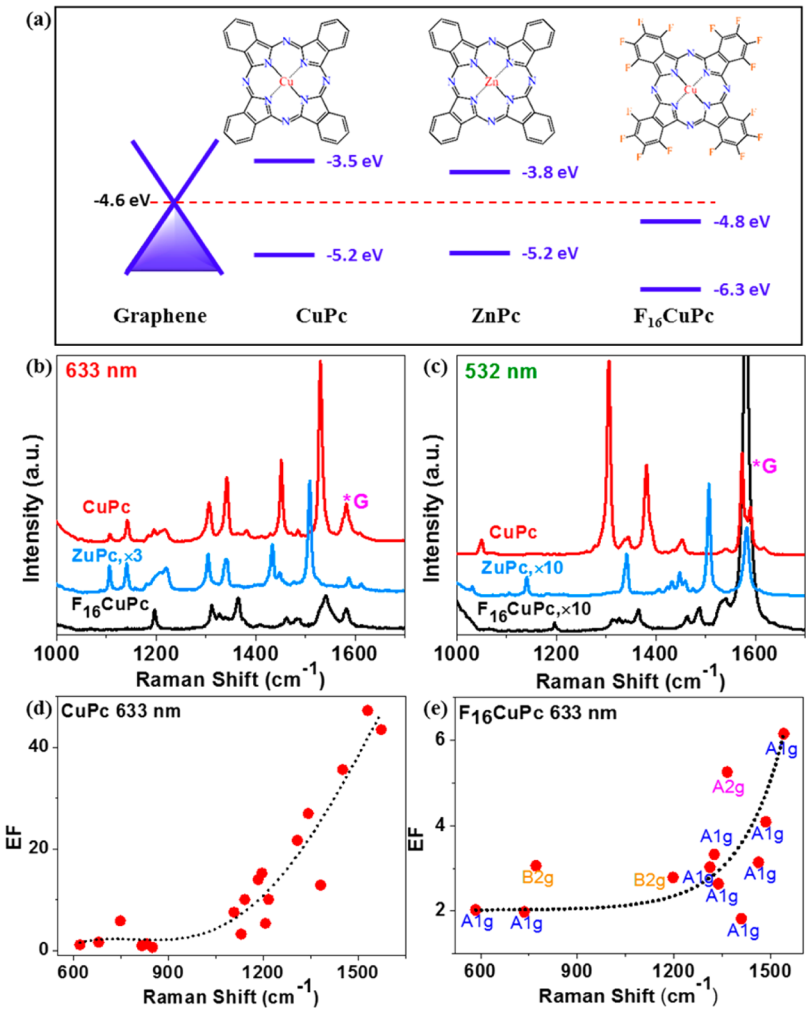

Figure 2. Influence of the molecular energy levels on GERS. (a) The first row shows the molecular structures of CuPc, ZnPc and F_{16}CuPc, from left to right. The second row shows the Dirac cone of graphene, the HOMO/LUMO energy levels of CuPc, ZnPc, and F_{16}CuPc. (b,c) Raman spectra of 2 Å CuPc (red line), 5 Å ZnPc (blue line), and 5 Å F_{16}CuPc (black line) on graphene using the excitation laser wavelengths of 633 nm (b) and 532 nm (c). The spectra are normalized with the intensities of their corresponding 1450 cm^{-1} peaks on the Si/SiO_2 substrate. The "*" marked peaks in (b,c) are the G-band from graphene. (d,e) The EF versus Raman shift for CuPc and F_{16}CuPc under 633 nm laser excitation. The red circles are experimental data and the black dotted curves are polynomial fits to the experimental data. (e) The symmetry assignment of each mode is also shown, labeled beside the data points. Different symmetries are labeled with different colors.

and therefore too small to ensure sufficient Raman scattering efficiency),[12,20] or the choice of an inappropriate excitation laser wavelength. In the case of low Raman cross sections, it is difficult to determine whether or not there is a Raman enhancement effect for these molecules on graphene. A full list of those molecules without observable Raman signals is shown in Table SI of the Supporting Information. In this work, we focus on molecules with large Raman cross sections and we study the effects of the molecular energy level and of the molecular symmetry on the GERS signal.

In the GERS system, the interaction strength between graphene and the molecule mainly depends on the degree of matching between the molecular energy levels and between the molecular symmetries with graphene. The Raman scattering intensity is strongly related to the energy band structures of the materials.[1,4,11,28] Figure 2 shows the Raman spectra of three molecules, CuPc, ZnPc, and F_{16}CuPc, on graphene that is supported by SiO_2/Si substrates. These three molecules have the same molecular structure (D_{4h} symmetry) with the only difference between them being in their metal ions (Cu^{2+} or Zn^{2+}) or the fluorine substituent (F^-) (Figure 2a). In addition, all of the molecules have planar structures, which allow for strong interactions with graphene. According to our DFT calculations shown in Table 1, upon adsorption on graphene these molecules share similar molecule−graphene separation distances (~3.2 Å) and adsorption energies (~−0.06 eV per atom), largely due to the similarity of their planar structures. However, their HOMO/LUMO energies are different, which are −5.2/−3.5 eV,[29] −5.2/−3.8 eV,[30] and −6.3/−4.8 eV,[31] respectively. Remarkable Raman enhancement has been observed for all of these three molecules on graphene using both 532 and 633 nm laser excitations, but the enhancement factors for them (the calculation of the GERS EF is described in Supporting Information) are very distinct, as seen in Figure 2b−e. For example, at 633 nm laser excitation the highest GERS EF of CuPc is 47.3 (at 1530 cm^{-1}), while the values are only 12.3 (at 1508 cm^{-1}) for ZnPc, and 6.2 (at 1540 cm^{-1}) for F_{16}CuPc. The EF at this vibrational mode of CuPc is 3.8 and 7.6 times larger than the EF of the same mode for ZnPc and F_{16}CuPc, respectively. These results indicate that despite their

DOI: 10.1021/nl5045988
Nano Lett. 2015, 15, 2892−2901

Table 1. List of Molecules with Strong and Weak GERS Effect, Including Their Structures (Related References in Superscript), Symmetries (Symm.), HOMO/LUMO levels, the Energy Differences between HOMO (or LUMO)[47] and Graphene's Fermi Level ($\Delta E_{HF}/\Delta E_{LF}$), the Typical Phonon Frequencies (ω_{ph}), and the Corresponding EFs under both 532 nm (Green Shaded) and 633 nm (Pink Shaded) Laser Excitation[b]

Molecule[Ref.]	Structure	Symm.	HOMO/LUMO (eV)	$\Delta E_{HF}/\Delta E_{LF}$ (eV)	d_z (Å)	E^{ads} (eV/atom)	ω_{ph} (cm^{-1})	EF
CuPc[29]	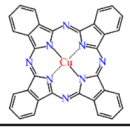	D_{4h}	-5.2/-3.5	-0.6/1.1	3.24	-0.06	1048 (532)[a] 1538 1451	37.5 11.6 24.3
							1530 (633) 1451	47.3 35.6
ZnPc[30]	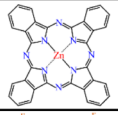	D_{4h}	-5.2/-3.8	-0.6/0.8	3.22	-0.06	1448 (532) 1508	4.1 11.9
							1508 (633) 1448	12.3 2.2
F_{16}CuPc[31]	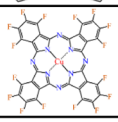	D_{4h}	-6.3/-4.8	-1.7/-0.2	3.19	-0.07	1540 (532) 1461	4.2 2.7
							1540 (633) 1461	6.2 3.1
PTCDA[30]		D_{2h}	-6.8/-4.7	-2.2/-0.1	3.17	-0.07	1532 (532) 1455	5.8 3.9
							1531 (633) 1454	8.3 3.9
TTP[38]	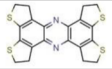	D_{2h}	-5.6/-2.3	-1.0/2.3	3.24	-0.07	1450 (633)	23.3
TCTA[39]	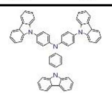	C_3	-5.7/-2.4	-1.1/2.2	4.34	-0.04	1340 (532) 1455	1.3 0.9
							1449 (633)	6.9
Sp2-NPB[40]	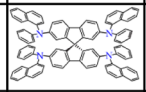	S_4	-5.5/-2.4	-0.9/2.2	4.36	-0.04	1503 (532) 1450	5.3 1.7
							1447 (633)	4.3
Sp2-TPD[42]	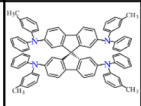	S_4	-5.5/-2.3	-0.9/2.3	4.27	-0.03	1450 (532) 1290	0.9 2.3
							1446 (633) 1290	0.9 1.0
TPBi[48]		C_3	-6.7/-2.7	-2.1/1.9			1450 (532) 1280	1 1.5
							1449 (633)	2.9
$Ir(ppy)_3$[47]		C_3	-5.6/-3.0	-1.0/1.6			none	
BCP[49]	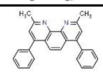	C_2	-7.0/-3.5	-2.4/1.1			1446 (633) (532 none)	1
Alq_3[49]		C_3	-5.8/-3.1	-1.2/1.5			none	

[a]Excitation wavelength in the units of nm. [b]The red horizontal line divides the molecules showing larger and smaller GERS EFs. For a molecule above the red line, DFT-calculated average molecule−graphene distance d_z, and the adsorption energy E^{ads} per atom of the molecule are listed as well (negative sign means energy release upon adsorption).

similar molecular structures, the presence of different molecular HOMO/LUMO levels plays an important role in GERS enhancement. Barros et al.[21] studied the relation between the GERS EF and other parameters, such as the graphene Fermi level, molecular HOMO/LUMO, phonon and laser energies. Using time-dependent perturbation theory for the Raman scattering process, they predicted that the energy levels of the molecule HOMO/LUMO are related to the GERS enhancement.[21] They found that strong GERS enhancement occurs when the phonon energy is close to the energy difference between the Fermi level of graphene and the HOMO/LUMO level of the molecules. Under such a condition, the GERS EF can be further increased if the laser energy is close to the HOMO−LUMO energy gap of the molecule. Figure 3 of ref 21 clearly illustrates the enhancement conditions, which are due to the better matching to the Raman resonance condition. In detail, according to eq 15 in ref 21, a large GERS EF can occur for the following four conditions

$$\hbar\omega_0 = \mathrm{LUMO} - \mathrm{HOMO} \quad \mathrm{OR}$$
$$\hbar\omega_0 = \mathrm{LUMO} - \mathrm{HOMO} + \hbar\omega_q \qquad \text{(i)}$$

$$E_F = \mathrm{HOMO} \pm \hbar\omega_q \quad \mathrm{OR} \quad E_F = \mathrm{LUMO} \pm \hbar\omega_q \qquad \text{(ii)}$$

DOI: 10.1021/nl5045988
Nano Lett. 2015, 15, 2892−2901

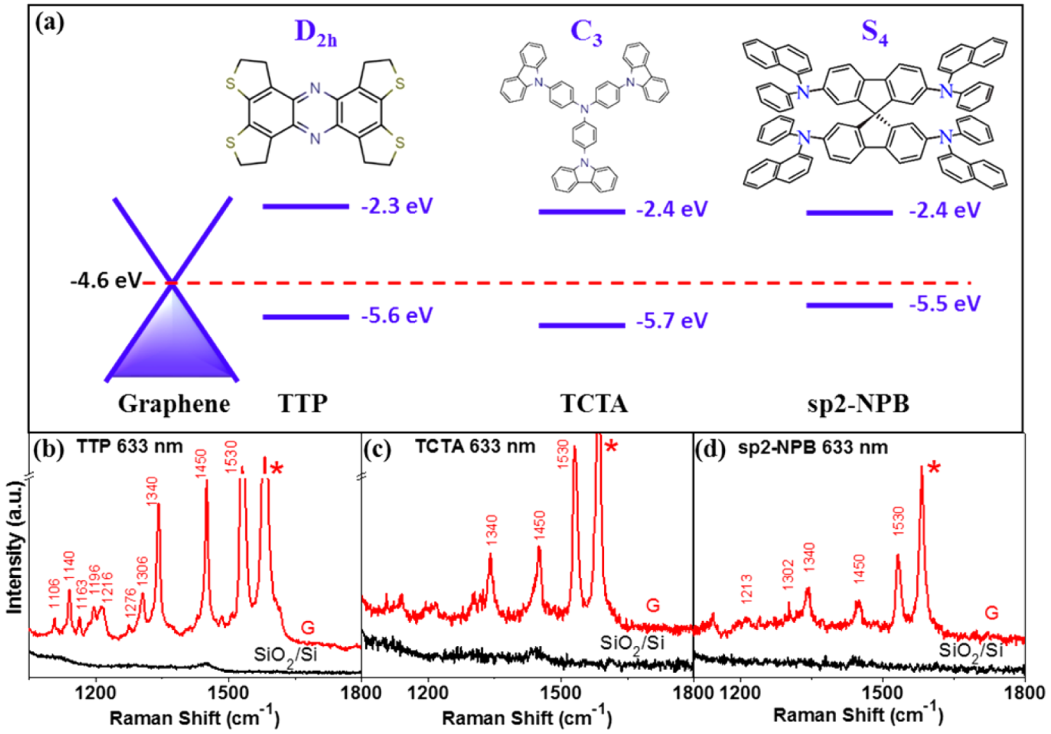

Figure 3. Influence of the molecular structure on GERS. (a) The first row shows the molecular structures of TCTA, TTP, and sp2-NPB molecules from left to right with labels above their corresponding Raman spectra with their symmetries labeled above. The second row shows the Dirac cone of graphene, the HOMO/LUMO energy levels of TCTA, TTP, and sp2-NPB. (b–d) Raman spectra of 5 Å (b) TTP, (c) TCTA, and (d) sp2-NPB, on graphene (red line) and on a blank SiO_2/Si substrate (black line) with the excitation laser wavelengths of 633 nm. The "*" marked peaks in (b–d) are the G-band from graphene. Other peaks marked by the numbers come from the corresponding molecules.

$$\hbar\omega_0 = E_F - \text{HOMO} \quad \text{OR}$$
$$\hbar\omega_0 = E_F - \text{HOMO} + \hbar\omega_q \qquad \text{(iii)}$$

$$\hbar\omega_0 = \text{LUMO} - E_F \quad \text{OR} \quad \hbar\omega_0 = \text{LUMO} - E_F - \hbar\omega_q \qquad \text{(iv)}$$

in which $\hbar\omega_0$ is the incident photon energy, $\hbar\omega_q$ is the phonon energy, and E_F is the graphene Fermi level. According to the perturbation theory treatment of Raman scattering and the Fermi's Golden Rule,[32] the Raman scattering efficiency is inversely proportional to the energy difference between the graphene Fermi level and the electronic levels of the molecule. Therefore, energy level matching in the molecule–graphene systems plays an important role in achieving a high GERS EF. It is worth mentioning that from a chemistry perspective, the scattering mechanism of the asymmetric modes in porphyrin-like molecules, including CuPc, ZnPc, and F_{16}CuPc here, is the Herzberg–Teller mechanism.[33−35] The model mentioned previously by Barros et al.[21] describes the scattering process from the perspective of time-dependent perturbation theory,[32] but it is also sufficient to reproduce and explain the increasing GERS EF trend with increased phonon frequency.

Our experimental results in Figure 2d show that the relation of EF vs phonon frequency of the CuPc molecule at 633 nm laser excitation matches the theoretical predictions in ref 21 and the analyses above, as confirmed in the polynomial fitting (black dotted curve) shown in Figure 2d. With the phonon frequency increasing from 600 cm^{-1} (0.07 eV) to 1600 cm^{-1} (0.20 eV), EF increases because the system is closer to the resonance condition, that is, the phonon energy equals the energy difference between the graphene Fermi level and the molecular HOMO/LUMO levels (eq ii above), or the phonon energy equals the energy difference between the laser energy and the HOMO–LUMO gap (eq i above). For CuPc under 532 nm laser excitation, the EFs are weaker than under 633 nm laser excitation, and the behavior (Figure S2(a) in the Supporting Information) does not match the theoretical prediction, as shown for the case of the 633 nm laser excitation, possibly because the 532 nm laser excitation is not in the resonance window with the HOMO/LUMO energy gap of CuPc. The phenomenon that EF increases with phonon frequency was also observed in F_{16}CuPc under 633 nm laser excitation (stronger than the 532 nm excitation because of the resonance excitation[36,37]), shown in Figure 2e. This mainly applies to the A_{1g} vibrational modes and may be due to the mode selection of the GERS enhancement mechanism.[12] The "Energy Level Rule" is successful for explaining most of the observation in Figure 2 and for the molecules with similar structure. But it is not complete, since it does not consider other factors (such as the molecular structure and the variety of the vibration) besides the energy level, which may induce different coupling strengths between graphene and the molecules too.

To investigate the molecular selection rule of GERS in terms of the molecular structure and symmetry, the molecules with similar HOMO/LUMO energy levels but with different molecular symmetries are chosen as probe molecules. TTP, TCTA, and sp2-NPB are three typical molecules with D_{2h}, C_3, and S_4 symmetry structures, respectively. They have similar HOMO/LUMO energy levels, as shown in Figure 3a. Their HOMO energy levels are at −5.5, −5.7, −5.6 eV,[38−40] respectively, and their LUMO energy levels are at −2.4, −2.4, −2.3 eV, respectively. Therefore, the difference between the

DOI: 10.1021/nl5045988
Nano Lett. 2015, 15, 2892−2901

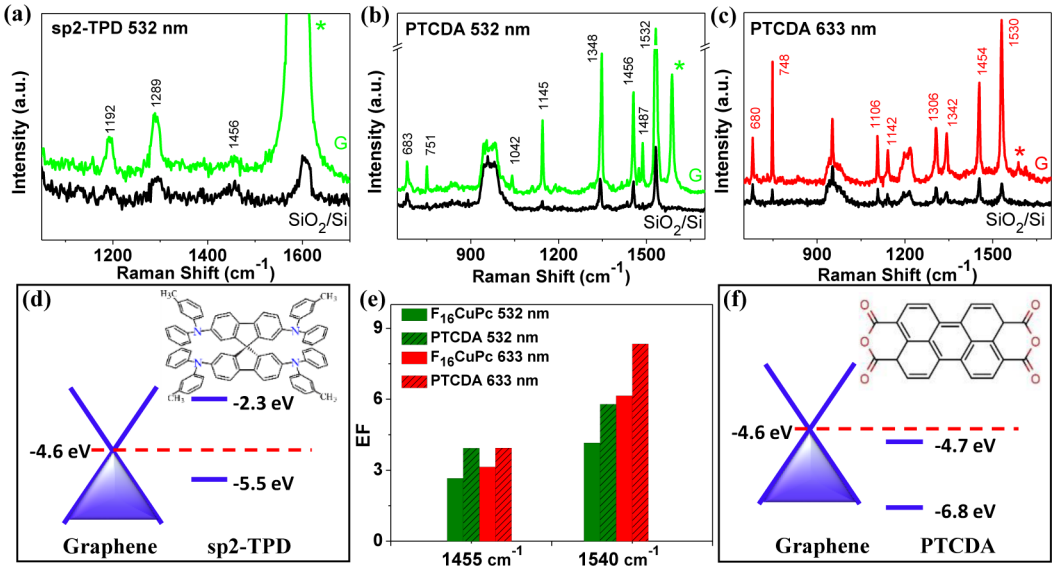

Figure 4. (a) Raman spectra of 5 Å sp2-TPD on graphene (colored line) and on a blank SiO_2/Si substrate (black line) taken with the excitation laser wavelength of 532 nm. (b,c) Raman spectra of 5 Å PTCDA on graphene (colored line) and on a blank SiO_2/Si substrate (black line) with the excitation laser wavelengths of 532 nm (b) and 633 nm (c), respectively. (d) The Dirac cone of graphene, and the HOMO/LUMO energy levels of sp2-TPD. The inset of (d) shows the molecular structure of sp2-TPD. (e) EF of two vibrational modes, 1455 and 1540 cm^{-1}, of F_{16}CuPc and PTCDA (dashed) under 532 nm (green) and 633 nm (red) laser excitations. (f) The Dirac cone of graphene, and the HOMO/LUMO energy levels of PTCDA. The inset of (f) shows the molecular structure of PTCDA. The "*" marked peaks in (a–c) are the G-band from graphene.

HOMO and LUMO energy levels does not contribute to the GERS EF and can be excluded as a distinguishing feature. Figure 3b–d shows the Raman spectra of these three molecules: TTP, TCTA and sp2-NPB, including both the Raman spectra of the molecules on graphene (red line) and on SiO_2/Si substrates (black line) under the 633 nm laser excitation. The corresponding results under the 532 nm laser excitation are shown in Figure S3 in the Supporting Information. It can be seen that the GERS EFs are different among these three molecules, which can be attributed to the influence of the molecular symmetry. Focusing on the 1450 cm^{-1} phonon mode, the distortion vibration of the 16-membered macrocycle and benzene ring,[36] the EFs of TTP, TCTA, and sp2-NPB under 633 nm excitation are about 23.3, 6.9, and 4.3, respectively. The EF of TTP is 3.4 and 5.4 times that for TCTA and sp2-NPB, respectively, indicating that the contribution of the molecular symmetry to the GERS effect follows the order $D_{2h} > C_3 > S_4$. TTP has a symmetry (D_{2h}) that matches best that of graphene (D_{6h}). The importance of this matching is built on the perturbation theory of Raman scattering,[32] which dictates that the Raman scattering intensity is positively correlated to the molecule–graphene coupling.[21]

To confirm the positive correlation between the GERS effect and molecule–graphene coupling, we carried out DFT calculations on the TTP, TCTA, and sp2-NPB molecules adsorbed on graphene. Contrary to TTP that has a planar structure, TCTA and sp2-NPB molecules prefer nonplanar geometries (see more details in Figure S7 in Supporting Information). Consequently, for TCTA and sp2-NPB the average molecule–graphene distance is more than 4.3 Å and the energy release upon adsorption is around 0.04 eV per atom, as shown in Table 1. However, TTP is much closer to the graphene substrate (~3.24 Å) and presents a noticeably larger energy release upon adsorption (0.07 eV per atom). Clearly, the molecule–graphene coupling is strongest for TTP, and thus it has the highest GERS EFs among these three molecules. From a chemistry perspective, it is likely that these molecules are scattered through the Franck–Condon mechanism.[41] In this regard, we can also learn that the GERS mechanisms of molecules in Figure 2 (CuPc, ZnPc, and F_{16}CuPc) and in Figure 3 (TTP, TCTA, sp2-NPB) are not the same. This is consistent with our analyses in this work: the GERS of molecules in Figure 2 can be attributed to the "Energy Level Rule" and that in Figure 3 can be attributed to the "Structure Rule". The usage of the Energy Level Rule and the Structure Rule can better and more straightforwardly reflect the relation between the molecule and graphene through a GERS process.

From the above discussion of the influence of the molecular symmetry, we conclude that the molecular symmetry influencing the GERS intensity operates mostly through the molecule–graphene coupling. Figure 4 provides an example in support of the importance of the coupling between the molecule and graphene. We selected the *N*,*N*′-bis(3-methylphenyl)-*N*,*N*′-diphenyl-9,9-spirobifluorene-2,7-diamine (sp2-TPD) molecule to compare with sp2-NPB. The GERS enhancement and energy levels of sp2-TPD are shown in Figure 4a,d, respectively. The HOMO/LUMO energies of sp2-TPD (Figure 4d) and sp2-NPB (Figure 3a) are almost identical with a difference of less than 0.1 eV.[42] In addition, these two molecules have the same structures, except for the substituents of $-CH_3$ in sp2-TPD and the parallel-connected conjugated benzene rings in sp2-NPB, shown in Figure 4d and Figure 3a, respectively. The slight structural difference leads to different GERS enhancement effects, as seen in Figure 4a and Figure 3d. Sp2-TPD does not have GERS enhancement under 633 nm laser excitation, but this enhancement is observable under 532 nm laser excitation. Sp2-NPB has GERS enhancement under both 633 and 532 nm excitations. In contrast, the 633 nm excitation yields stronger effects, including more molecular Raman peaks being resolved with observable intensities. Comparing these two molecules, sp2-NPB has a stronger GERS enhancement effect than sp2-TPD, where under 532 nm

DOI: 10.1021/nl5045988
Nano Lett. 2015, 15, 2892–2901

excitation the phonon mode at 1450 cm^{-1} has an EF of 1.7 for sp2-NPB but only 0.9 for sp2-TPD, which is a factor of 2 lower.

This observation of different GERS EFs between sp2-TPD and sp2-NPB might be explained by the relatively weak coupling between sp2-TPD and graphene. For sp2-NPB, the parallel-connected conjugated benzene rings could strengthen the coupling between the molecule and graphene because of the similarities between graphene's hexagonal carbon lattice and the benzene rings. Such an enhanced molecular−graphene coupling does not exist for sp2-TPD, where no parallel-connected conjugated benzene ring but $-CH_3$ substituents make up the molecular structure. Our DFT calculations also indicate that sp2-NPB has a slightly higher energy release upon adsorption (0.04 eV per atom) than sp2-TPD (0.03 eV per atom), as shown in Table 1. So the relatively weaker coupling possibly gives the overall smaller GERS enhancement in sp2-TPD than in sp2-NPB.

The effect of the molecule−graphene coupling can be strong in the GERS enhancement effect. In particular, the existence of connected benzene rings helps to strengthen the coupling and thus helps to enhance the GERS enhancement effect. To further confirm this hypothesis, we selected the molecule 3,4,9,10-perylene-tetracarboxylicacid-dianhydride (PTCDA) for GERS measurement, as shown in Figure 4(b,c,e,f). In terms of the HOMO/LUMO levels, F_{16}CuPc and PTCDA have similar LUMO energies that are only 0.1 eV different from each other, and PTCDA has a HOMO energy 0.5 eV lower than that of F_{16}CuPc.[30] The HOMO/LUMO gaps are therefore 2.1 eV for PTCDA and 1.5 eV for F_{16}CuPc. PTCDA is not resonant under 633 nm laser excitation[43] but its GERS EFs are mostly larger for 633 nm laser excitation than for 532 nm laser excitation. This could be possibly attributed to the strong PTCDA−graphene coupling. The small energy difference of graphene's Fermi energy and the LUMO of PTCDA results in an effective charge transfer between graphene and PTCDA and therefore results in the shifts of these energy levels. In addition, the seven parallel-connected conjugated rings of PTCDA, also with D_{2h} symmetry, make the molecule−graphene distance small (3.17 Å in Table 1) and the coupling between graphene and PTCDA strong (E^{ads} around −0.07 eV per atom).

Compared to PTCDA, F_{16}CuPc has a similar HOMO level and a smaller HOMO/LUMO energy gap that makes it easier for the 633 nm laser to yield strong Raman scattering. The GERS EFs of F_{16}CuPc and PTCDA are similar with slightly higher EF values for PTCDA. Take the 1540 cm^{-1} phonon mode (the C−C stretching vibration on the benzene and pyrrole ring[44]) as an example. Under 532 nm laser excitation, the EFs of F_{16}CuPc and PTCDA are 4.2 and 5.8, respectively. Under 633 nm laser excitation, the EFs of F_{16}CuPc and PTCDA are 6.2 and 8.3, respectively. For the 1450 cm^{-1} phonon mode, under 532 nm laser excitation the EFs of F_{16}CuPc and PTCDA are 2.7 and 3.9, respectively; under 633 nm laser excitation, the EFs of F_{16}CuPc and PTCDA are 3.1 and 3.9, respectively. For both of these vibrational modes, the GERS EFs for PTCDA are about 1.4 times that for F_{16}CuPc under both 532 and 633 nm laser excitations, shown in Figure 4e. Compared to the large GERS EF differences between CuPc, ZnPc, and F_{16}CuPc or between TTP, TCTA, and sp2-NPB, the EF difference between F_{16}CuPc and PTCDA is relatively small, which can be attributed to their similar molecule−graphene distance and coupling. The slightly stronger GERS enhancement of PTCDA could be partly due to the parallel-connected conjugated ring structure of PTCDA and thus the relatively smaller PTCDA−graphene distance (see Table 1),[45] which is important to strengthen the coupling between the molecule and its graphene substrate. This strengthened coupling with graphene due to conjugated-rings, which has been reported before,[46] might result in a shift of the molecular HOMO/LUMO energy levels. Overall, these experimental observations suggest that the GERS EF is increased with the smaller distance and stronger coupling between the molecules and graphene.

We can now summarize our findings with the establishment of a set of rules for the molecular selectivity of the GERS enhancement process. Table 1 summarizes results obtained for 12 molecules. The table includes their structures, symmetries, HOMO/LUMO energies,[47] the energy differences between the HOMO/LUMO and the graphene Fermi energy (ΔE_{HF}, ΔE_{LF}), molecule−graphene distance (d_z), adsorption energy (E^{ads}), typical phonon modes (ω_{ph}), and the corresponding EFs. In this table, TPBi, iridium, tris(2-phenylpyidine) ($Ir(ppy)_3$), BCP, and tris(8-hydroxyquinoline) aluminum (Alq_3) all show very small or no GERS enhancement under 532 or 633 nm laser excitations. From the other molecules, it is clear to see that the GERS effect follows the molecular selectivity rules as below: (1) Energy Level Rule. GERS enhancement requires the appropriate HOMO/LUMO energy levels of the molecules with a certain energy laser excitation (eqs i−iv). Briefly, strong enhancement occurs when the HOMO/LUMO differs from the graphene Fermi Level by the phonon energy. Further enhancement can occur when the excitation laser energy is close to the molecular HOMO/LUMO energy separation. The different GERS EF values of CuPc, ZnPc, and F_{16}CuPc support this rule, because these molecules have similar molecule−graphene coupling but different HOMO/LUMO values. As another example, TPBi and BCP have HOMO/LUMO gaps of 4[48] and 3.5 eV,[49] which are too large to be resonant with the 532 or 633 nm laser. Their HOMO/LUMO energies are also too far away from the graphene Fermi energy, possibly leading to a weak charge transfer between the molecule and graphene. This may be part of the reason why no GERS effects were observed for these molecules under 532 or 633 nm excitation. (2) Structure Rule. Molecular structure with D_{nh} symmetry is favorable for GERS enhancement. A strong molecule−graphene coupling, which helps GERS enhancement, requires a small molecule−graphene distance and a structural match of the molecules and graphene. D_{nh} symmetry of the molecule is a good condition for structural compatibility. Symmetry matching leads to the stronger GERS effect for Pc derivatives, PTCDA, and TTP molecules, which have the symmetry of D_{4h}, D_{2h}, and D_{2h}, respectively, and a weaker GERS effect is seen for sp2-NPB and sp2-TPD with S_4 symmetry. Molecules TPBi, $Ir(ppy)_3$, BCP, and Alq_3, each of which has the symmetry of C_3, C_3, C_2, and C_3, respectively, have nonplanar structures.[48−50] Such low symmetries and nonplanar structures could also lead to their weak molecule−graphene couplings and contribute to the weak GERS enhancement effects of these four molecules. Additionally, parallel-connected conjugated rings in the molecular structure are favorable in obtaining strong GERS enhancement, because the connected rings increase the structural similarity between the molecule and graphene, and therefore generally reduce the molecule−graphene distance and strengthen the coupling. The stronger enhancements of TTP (compared to TCTA) and sp2-NPB (compared to sp2-TPD) support this rule of ring-connection and molecule−graphene coupling. Because of the different molecule−graphene interactions, the same vibrational mode

DOI: 10.1021/nl5045988
Nano Lett. 2015, 15, 2892−2901

shows different GERS EFs in different molecules. For example, the 1450 cm^{-1} vibrational mode under 633 nm laser excitation has a GERS EF ranging from 0.9 (in sp2-TPD) to 35.6 (in CuPc); for the 1530 cm^{-1} mode under 633 nm laser excitation, the GERS EF can range from 6.2 (in F_{16}CuPc) to 47.3 (in CuPc). This broad variation of the GERS EF for the same vibrational mode demonstrates the strong effect of the molecular selectivity in GERS. From Table 1, we conclude that a strong GERS EF requires the appropriate HOMO/LUMO levels for the molecule and the molecular symmetry and structure to be well matched with graphene to maximize the molecule−graphene coupling.

To further support the finding that the molecules with a strong GERS effect are strongly coupled with graphene, we performed a set of UV−visible absorption measurements for different molecules with and without contacting the graphene substrates (Figure 5). The molecules chosen here include

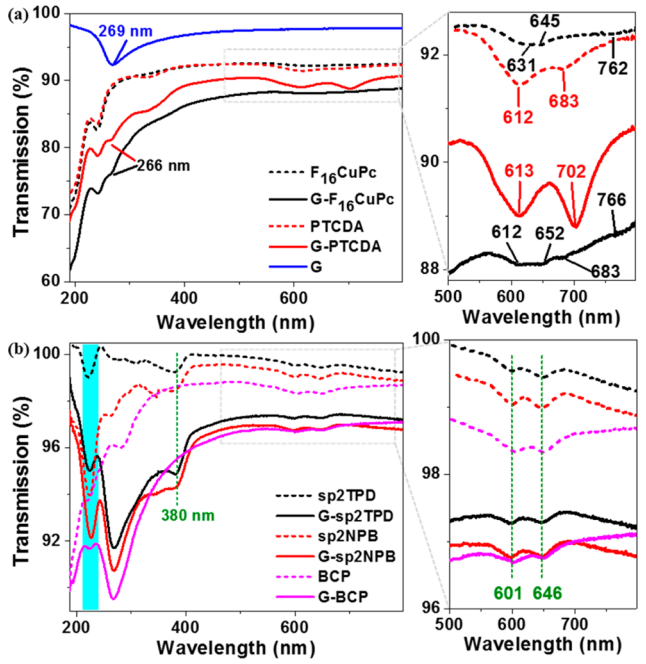

Figure 5. (a) The UV−vis transmission spectra of pristine graphene (blue solid line), F_{16}CuPc (black dashed line), F_{16}CuPc on graphene (black solid line), PTCDA (red dashed line), and PTCDA on graphene (red solid line). The enlarged spectra of (a) in the wavelength range of 500−800 nm are shown on the right. The wavelengths of the transmission valleys (absorption peaks) are labeled, including the graphene π-band at approximately 270 nm. (b) The UV−vis transmission spectra of sp2-TPD (black dashed line) and sp2-TPD on graphene (black solid line), sp2-NPB (red dashed line) and sp2-NPB on graphene (red solid line), BCP (magenta dashed line) and BCP on graphene (magenta solid line). The wavelengths of the transmission valleys (absorption peaks) are labeled with a green dotted line and a cyan box. The enlarged spectra of (b) in the wavelength range of 500 to 800 nm are shown on the right of (b).

F_{16}CuPc and PTCDA (Figure 5a), which have large GERS EFs, and sp2-TPD, sp2-NPB, and BCP (Figure 5b), which have small or no GERS EFs. As seen in Figure 5a, the absorption of graphene's π-band at 269 nm is obvious, indicating the good crystal quality of graphene. For all the molecules in Figure 5, the light absorptions are stronger when the molecules are deposited on graphene, suggesting the role of graphene in absorbing light. For F_{16}CuPc and PTCDA, molecular absorption peaks are also frequency shifted when molecules contact graphene. Upon contact to graphene, F_{16}CuPc presents absorption peaks at 631 and 645 nm that split into three peaks, 612, 652, and 683 nm, and the absorption peak at 762 nm that red shifts to 766 nm. For PTCDA, the absorption peak at 612 nm does not show an observable frequency shift when PTCDA is on graphene, but the peak at 683 nm is red shifted by almost 20 nm. Graphene's π-band at 269 nm is also blue shifted to 266 nm when graphene contacts F_{16}CuPc or PTCDA. These phenomena suggest that the interaction between molecules and graphene, and the different UV−visible absorption changes between F_{16}CuPc and PTCDA demonstrate the different levels of the molecule−graphene interactions of these two molecules. Besides F_{16}CuPc and PTCDA, CuPc also shows its coupling with graphene and this conclusion is supported by the UV−visible absorption change before and after contacting graphene,[51] which shows an additional strong absorption peak at 706 nm when CuPc is on graphene. Compared to F_{16}CuPc and PTCDA, the molecules with a small GERS EF, that is, sp2-TPD, sp2-NPB and BCP, do not show frequency shifts in their absorption peaks near 601 and 646 nm for all three molecules and at approximately 380 nm for sp2-TPD and sp2-NPB. For the absorption peaks near 220 nm for sp2-TPD and sp2-NPB, slight frequency shifts appear when these molecules are on graphene: a red shift of 3 nm for the 223 nm peak (without graphene) of sp2-NPB and a red shift of 3 nm for the 221 nm peak of sp2-TPD. These slight frequency shifts suggest the weak coupling between graphene and these molecules, and this weak coupling is also reflected in the small GERS EF (less than 5). In contrast, no frequency shift in the absorption peak near 220 nm can be observed for the case of the BCP molecule, suggesting that graphene has an even weaker interaction with BCP than with sp2-NPB and sp2-TPD. This weaker interaction can also be demonstrated in the GERS EF in which BCP's GERS EF is nearly 1, which is smaller than the values of sp2-TPD and sp2-NPB. Figure S4 in the Supporting Information also shows the UV−visible spectra of TPBi, which has a low GERS EF and is similar to the situation of sp2-TPD and sp2-NPB. Moreover, sp2-NPB has larger light absorption than sp2-TPD in the visible range. The absorption differences between these two molecules ($\Delta\alpha_M = \alpha_{M1} - \alpha_{M2}$, where α_{M1} and α_{M2} are the absorptions of the two molecules, respectively) are not the same at wavelengths of 532 and 633 nm, and the difference of $\Delta\alpha_M$ between 532 and 633 nm light, $\Delta\alpha_{M,wl} = |\Delta\alpha_{M,532\ nm} - \Delta\alpha_{M,633\ nm}|$, becomes larger after the molecules come into contact with the graphene surface. As shown in Figure 5, before being placed in contact with graphene, their light absorption differences ($\Delta\alpha_M$) are 0.42% at 532 nm and 0.44% at 633 nm, resulting in $\Delta\alpha_{M,wl}$ of 0.02%. After contacting the graphene surface, the absorption differences ($\Delta\alpha_{M,on\ G}$) become 0.41% at 532 nm and 0.51% at 633 nm, resulting in $\Delta\alpha_{M,on\ G,wl}$ of 0.10%. The fact that $\Delta\alpha_{M,wl} \neq \Delta\alpha_{M,on\ G,wl}$ also shows the different strengths of the molecule−graphene coupling for sp2-NPB and sp2-TPD. Besides the difference in their adsorption energies E^{ads} shown in Table 1, the difference in light absorbance at different wavelengths may be another factor that contributes to their different Raman intensities with different excitation laser wavelengths.

Conclusion. In conclusion, we have studied the molecular selectivity of GERS through systematic experimental measurements on a number of representative molecules. The experimental data were complemented with first-principles calculations to extract two general basic rules for strong GERS

DOI: 10.1021/nl5045988
Nano Lett. 2015, 15, 2892−2901

enhancement. First, we established that molecules should have the appropriate HOMO/LUMO energy level alignments. This rule is theoretically analyzed using third order perturbation theory in the application of Raman scattering and is demonstrated by the GERS enhancement of the CuPc molecule. Second, the molecule's structure must display an appropriate point group symmetry, including D_{nh} symmetry, and parallel-connected conjugated rings in their structures. The former condition is a basic requirement for a strong molecule−graphene structural compatibility and interaction that yields a stronger charge-transfer and a larger GERS EF. The latter is an additional requirement for the molecule−graphene structural compatibility that has to be fulfilled in addition to the D_{nh} symmetry. Such parallel-connected rings, which are similar to graphene's hexagonal lattice structure, are important for both molecule−graphene coupling and charge transfer, and both factors can enhance the GERS EF. Both selection rules of the molecular energy levels and of the molecular structure cooperate to achieve a strong molecular−graphene interaction, and therefore an effective charge-transfer between the molecules and graphene. This requirement of molecule−graphene interaction was also supported by the UV−visible absorption spectra measurements before and after contact with the graphene substrate. Considerable frequency shifts are observed for molecules with large GERS EF, and negligible frequency shifts are observed for those molecules showing a small GERS EF. This work is important for the study of the chemical mechanism for the SERS effect, and more generally for the study of molecule−graphene coupling. Moreover, GERS has many applications in the areas of chemical or biological sensing, and our work points out how to choose the right molecules in GERS measurements for different applications. Therefore, this work offers useful guidelines for the applications of the GERS effect in chemical detection, as well as for the potential GERS effect application in medical and biological technologies.

Method. *Experimental Methods.* The graphene substrates were prepared by mechanical exfoliation. Monolayer flakes are identified under the optical microscope (Axio Imager, Carl Zeiss) and further analyzed using the atomic force microscope (AFM, Dimension 3100, Veeco Instruments Inc.) and Raman spectroscopy. All Raman spectra were taken using a Horiba Jobin-Yvon HR800 Raman spectrometer. The excitation wavelengths for the measurement were typically 532 and 633 nm. The laser power on the samples was about 1 mW. A 100× objective was used to focus the laser beam. The spectral parameters were obtained by fitting the peaks using a Lorentzian/Gaussian line shape.

For the UV−visible absorption measurement, CVD (chemical vapor deposition) monolayer graphene was transferred onto a quartz substrate using PMMA prior to molecular evaporation. The UV−visible measurement was performed using a Cary 5000 UV−visible-NIR Dual-Beam spectrometer operating in the transmission mode. The blank quartz substrate was used as a background reference.

The molecules were deposited on the substrates using a thermal evaporator. The base pressure for deposition was about 10^{-6} Torr. For Raman spectra measurements, the deposition thicknesses are 2 Å for CuPc and 5 Å for other molecules. For the UV−visible absorption measurement, the deposition thicknesses are 5 Å for all molecules. The molecule thicknesses were monitored by a quartz crystal. The thicknesses of the molecules in our work guaranteed submonolayer coverage of molecules,[52] ensuring that all the molecules on the graphene surface are affected by graphene to increase the accuracy of the measured GERS EFs.

XPS (X-ray photoelectron spectroscopy) measurements are further performed to prove that the molecule coverage is uniform on the sample surface, and that the numbers of molecule on a blank SiO_2/Si substrate and on graphene are the same. Details about the XPS measurements and error analysis are provided in Supporting Information. Considering a molecule with the size of 2 nm in diameter and assuming that the molecules covered the graphene surface exactly in the monolayer, the number of molecules in the focused spot of the excitation laser (~1 μm in diameter) is estimated to be in the order of 10^5.

Theoretical Calculations. Plane-wave DFT calculations were performed using the VASP package[53] within the generalized gradient approximation using the Perdew−Burke−Ernzerhof exchange-correlation functional.[54] The optB86b-vdW functional was used to account for the vdW interaction between the molecule and graphene substrate.[55] The projector augmented wave pseudopotentials were used with a cutoff energy set at 400 eV. For graphene, its orthorhombic unit cell has in-plane lattice constants of about 4.26 Å (along the armchair direction) and 2.46 Å (along the zigzag direction). The z-lattice constant was set as 24.00 Å to avoid spurious interactions with replicas. Then the graphene substrate was built by a periodic slab geometry[56] with a 7 × 12 × 1 supercell (the size as 29.82 Å × 29.52 Å × 24.00 Å) to ensure at least 14 Å vacuum spacings in all directions for the molecule adsorbed on the graphene. The supercell is large enough so that a single k-point at the Gamma point of the Brillouin zone is sufficient for the k-point sampling. For the molecule−graphene system, all atoms were relaxed until the residual forces were below 0.02 eV/Å.

■ ASSOCIATED CONTENT

Ⓢ Supporting Information

Molecules with small Raman cross sections; the calculation of GERS EF and its error; GERS EF of CuPc, ZnPc, and F_{16}CuPc; laser energy dependence of GERS; UV−visible absorption spectra of TPBi; uniformity of molecule coverage on sample surface; atomic structures of nonplanar TCTA and NPB molecules This material is available free of charge via the Internet at http://pubs.acs.org.

■ AUTHOR INFORMATION

Corresponding Authors

*E-mail: millie@mgm.mit.edu. Tel: +1-617-253-6864.
*E-mail: xiling@mit.edu. Tel: +1-617-253-6860.

Author Contributions

S.H. and X.L. contributed equally to this work.

S.H., X.L., J.Z., and M.S.D. designed the experiment. S.H. and X.L. conducted the sample preparation, spectroscopy measurement, and other characterizations. Y.S., W.F., and J.K. contributed to the CVD growth of graphene. L.L. and V.M. contributed to the theoretical calculation. S.H. and X.L. analyzed the data. S.H. and X.L. cowrote the paper. All the authors discussed the results and revised the paper.

Notes

The authors declare no competing financial interest.

DOI: 10.1021/nl5045988
Nano Lett. 2015, 15, 2892−2901

■ ACKNOWLEDGMENTS

This work is partially supported by the National Science Foundation under award number NSF/DMR 1004147 and by NSFC (21233001, 21129001). The work at Rensselaer Polytechnic Institute (RPI) was supported by New York State under NYSTAR program C080117 and the Office of Naval Research. The computations were performed using the resources of the Center for Computational Innovation at RPI. W.F. and J.K. acknowledge the support through the STC Center for Integrated Quantum Materials from NSF (U.S.) grant DMR-1231319..

■ REFERENCES

(1) Campion, A.; Kambhampati, P. *Chem. Soc. Rev.* **1998**, *27*, 241−250.
(2) Albrecht, M. G.; Creighton, J. A. *J. Am. Chem. Soc.* **1977**, *99*, 5215−5217.
(3) Jeanmaire, D. L.; Van Duyne, R. P. *J. Electroanal. Chem. Interfacial Electrochem.* **1977**, *84*, 1−20.
(4) Kneipp, K.; Moskovits, M.; Kneipp, H. *Surface-Enhanced Raman Scattering: Physics and Applications*; Springer-Verlag: Berlin Heidelberg, 2006.
(5) Tian, Z.-Q.; Ren, B.; Wu, D.-Y. *J. Phys. Chem. B* **2002**, *106*, 9463−9483.
(6) Ren, B.; Huang, Q. J.; Cai, W. B.; Mao, B. W.; Liu, F. M.; Tian, Z. Q. *J. Electroanal. Chem.* **1996**, *415*, 175−178.
(7) Schatz, G.; Young, M.; Van Duyne, R. P. *Surf. Enhanced Raman Scattering* **2006**, *103*, 19−45.
(8) *Topics in Applied Physics*; Otto, A., Futamata, M., Kneipp, K., Moskovits, M., Kneipp, H., Eds.; Springer: Berlin Heidelberg, 2006; pp 147−182.
(9) Le Ru, E. C.; Blackie, E.; Meyer, M.; Etchegoin, P. G. *J. Phys. Chem. C* **2007**, *111*, 13794−13803.
(10) Morton, S. M.; Jensen, L. *J. Am. Chem. Soc.* **2009**, *131*, 4090−4098.
(11) Campion, A.; Ivanecky, J. E.; Child, C. M.; Foster, M. *J. Am. Chem. Soc.* **1995**, *117*, 11807−11808.
(12) Ling, X.; Xie, L.; Fang, Y.; Xu, H.; Zhang, H.; Kong, J.; Dresselhaus, M. S.; Zhang, J.; Liu, Z. *Nano Lett.* **2010**, *10*, 553−561.
(13) Ling, X.; Moura, L. G.; Pimenta, M. A.; Zhang, J. *J. Phys. Chem. C* **2012**, *116*, 25112−25118.
(14) Ling, X.; Wu, J.; Xie, L.; Zhang, J. *J. Phys. Chem. C* **2013**, *117*, 2369−2376.
(15) Ling, X.; Zhang, J. *Small* **2010**, *6*, 2020−2025.
(16) Ling, X.; Wu, J.; Xu, W.; Zhang, J. *Small* **2012**, *8*, 1365−1372.
(17) Xu, H.; Xie, L.; Zhang, H.; Zhang, J. *ACS Nano* **2011**, *5*, 5338−5344.
(18) Wang, Y.; Li, Z.; Wang, J.; Li, J.; Lin, Y. *Trends Biotechnol.* **2011**, *29*, 205−212.
(19) Zhao, Y.; Xie, Y.; Bao, Z.; Tsang, Y. H.; Xie, L.; Chai, Y. *J. Phys. Chem. C* **2014**, *118*, 11827−11832.
(20) Ru, E. Le; Etchegoin, P. *Principles of Surface-Enhanced Raman Spectroscopy: and Related Plasmonic Effects*; Elsevier: New York, 2008; pp 55−57.
(21) Barros, E. B.; Dresselhaus, M. S. *Phys. Rev. B* **2014**, *90*, 035443.
(22) Austin, L. A.; Kang, B.; Yen, C.-W.; El-Sayed, M. A. *Bioconjugate Chem.* **2011**, *22*, 2324−2331.
(23) Liu, Q.; Zhou, Q.; Jiang, G. *TrAC, Trends Anal. Chem.* **2014**, *58*, 10−22.
(24) Jiao, S.; Wang, Y.; Chen, C.; Wu, X.; Bei, F. *J. Mol. Struct.* **2014**, *1062*, 48−52.
(25) Lin, D.; Qin, T.; Wang, Y.; Sun, X.; Chen, L. *ACS Appl. Mater. Interfaces* **2014**, *6*, 1320−1329.
(26) Xu, W.; Ling, X.; Xiao, J.; Dresselhaus, M. S.; Kong, J.; Xu, H.; Liu, Z.; Zhang, J. *Proc. Natl. Acad. Sci. U.S.A.* **2012**, *109*, 9281−9286.
(27) Manikandan, M.; Nasser Abdelhamid, H.; Talib, A.; Wu, H.-F. *Biosens. Bioelectron.* **2014**, *55*, 180−186.
(28) Kneipp, K.; Kneipp, H.; Itzkan, I.; Dasari, R. R.; Feld, M. S. *J. Phys.: Condens. Matter* **2002**, *14*, R597−R624.
(29) Chu, C.-W.; Shrotriya, V.; Li, G.; Yang, Y. *Appl. Phys. Lett.* **2006**, *88*, 153504.
(30) Schlaf, R.; Parkinson, B. A.; Lee, P. A.; Nebesny, K. W.; Armstrong, N. R. *J. Phys. Chem. B* **1999**, *103*, 2984−2992.
(31) Shen, C.; Kahn, A.; Schwartz, J. *J. Appl. Phys.* **2001**, *90*, 6236.
(32) Jorio, A.; Saito, R.; Dresselhaus, G.; Dresselhaus, M. S. *Raman Spectroscopy in Graphene Related Systems*; Wiley-VCH: New York, 2011.
(33) Yang, P.; Qi, D.; You, G.; Shen, W.; Li, M.; He, R. *J. Chem. Phys.* **2014**, *141*, 124304.
(34) Santoro, F.; Lami, A.; Improta, R.; Bloino, J.; Barone, V. *J. Chem. Phys.* **2008**, *128*, 224311.
(35) Corio, P.; Rubim, J. C.; Aroca, R. *Langmuir* **1998**, *14*, 4162−4168.
(36) Cerdeira, F.; Garriga, M.; Alonso, M. I.; Ossó, J. O.; Schreiber, F.; Dosch, H.; Cardona, M. *J. Raman Spectrosc.* **2013**, *44*, 597−607.
(37) Wu, F.-C.; Cheng, H.-L.; Yen, C.-H.; Lin, J.-W.; Liu, S.-J.; Chou, W.-Y.; Tang, F.-C. *Phys. Chem. Chem. Phys.* **2010**, *12*, 2098−2106.
(38) Xie, Y.; Fujimoto, T.; Dalgleish, S.; Shuku, Y.; Matsushita, M. M.; Awaga, K. *J. Mater. Chem. C* **2013**, *1*, 3467.
(39) Hung, W.-Y.; Tu, G.-M.; Chen, S.-W.; Chi, Y. *J. Mater. Chem.* **2012**, *22*, 5410.
(40) New, E.; Howells, T.; Sullivan, P.; Jones, T. S. *Org. Electron.* **2013**, *14*, 2353−2359.
(41) Guo, M.; He, R.; Dai, Y.; Shen, W.; Li, M.; Zhu, C.; Lin, S. H. *J. Chem. Phys.* **2012**, *136*, 144313.
(42) Scholz, R.; Gisslén, L.; Himcinschi, C.; Vragović, I.; Calzado, E. M.; Louis, E.; San Fabián Maroto, E.; Díaz-García, M. A. *J. Phys. Chem. A* **2009**, *113*, 315−324.
(43) Kobitski, A. Y.; Salvan, G.; Scholz, R.; Tenne, D.; Kampen, T. U.; Wagner, H. P.; Zahn, D. R. T. *Appl. Surf. Sci.* **2002**, *190*, 386−389.
(44) Basova, T.; Kolesov, B. *J. Struct. Chem.* **2000**, *41*, 770−777.
(45) Martínez-Galera, A. J.; Nicoara, N.; Martínez, J. I.; Dappe, Y. J.; Ortega, J.; Gómez-Rodríguez, J. M. *J. Phys. Chem. C* **2014**, *118*, 12782−12788.
(46) Huang, C.; Kim, M.; Wong, B. M.; Safron, N. S.; Arnold, M. S.; Gopalan, P. *J. Phys. Chem. C* **2014**, *118*, 2077−2084.
(47) http://www.sigmaaldrich.com/materials-science/.
(48) Takizawa, S.; Montes, V. A.; Anzenbacher, P. *Chem. Mater.* **2009**, *21*, 2452−2458.
(49) Cheng, J.-A.; Chen, C. H. *J. Mater. Chem.* **2005**, *15*, 1179.
(50) Gao, H.; Qin, C.; Zhang, H.; Wu, S.; Su, Z.-M.; Wang, Y. *J. Phys. Chem. A* **2008**, *112*, 9097−9103.
(51) Ling, X.; Fang, W.; Lee, Y.-H.; Araujo, P. T.; Zhang, X.; Rodriguez-Nieva, J. F.; Lin, Y.; Zhang, J.; Kong, J.; Dresselhaus, M. S. *Nano Lett.* **2014**, *14*, 3033−3040.
(52) Gorgoi, M.; Michaelis, W.; Kampen, T. .; Schlettwein, D.; Zahn, D. R. . *Appl. Surf. Sci.* **2004**, *234*, 138−143.
(53) Kresse, G.; Furthmüller, J. *Comput. Mater. Sci.* **1996**, *6*, 15−50.
(54) Perdew, J. P.; Burke, K.; Ernzerhof, M. *Phys. Rev. Lett.* **1996**, *77*, 3865−3868.
(55) Liang, L.; Wang, J.; Lin, W.; Sumpter, B. G.; Meunier, V.; Pan, M. *Nano Lett.* **2014**, *14*, 6400−6406.
(56) Liang, L.; Meunier, V. *Phys. Rev. B* **2012**, *86*, 195404.

DOI: 10.1021/nl5045988
Nano Lett. 2015, 15, 2892−2901